JOURNAL OF THERMOPHYSICS AND HEAT TRANSFER
Vol. 21, No. 1, January–March 2007

Application of an *hp*-Adaptive FEM for Solving Thermal Flow Problems

Xiuling Wang* and Darrell W. Pepper†
University of Nevada, Las Vegas, Las Vegas, Nevada 89154

DOI: 10.2514/1.22414

Numerical results are presented for a set of forced and natural convective problems using an *hp*-adaptive finite element technique. The *hp*-adaptive model is based on mesh refinement and increasing spectral order to produce enhanced accuracy while reducing computational requirements. An a posteriori error estimator based on the L_2 norm is employed to guide the adaptation procedure. A projection algorithm is employed as the flow solver. Example test cases consisting of natural convection in a differentially heated enclosure, flow with forced convection over a backward facing step and natural convection within an enclosed partition are presented. Numerical results compare closely with published data.

Nomenclature

A = advection matrix
B = body force
C = gradient operator
e = error
F_v = load vector for velocity
F_T = load vector for temperature
g = gravity
h = element size
h_e = characteristic element length
K_v = diffusion matrix for velocity
K_T = diffusion matrix for temperature
k_h = diffusion coefficient
L = linear orthogonal projection operator
M = mass matrix
m = total element number
N_i = shape function
P = pressure
Pr = Prandtl number
Pe = Peclet number
p = shape function order
Re = Reynolds number
Ra = Rayleigh number
T = temperature
t = time
V = velocity vector
W_i = Petrov–Garlerkin weighted function
x = dimensional space (x, y)
α = thermal diffusivity, Petrov–Galerkin weighting factor
β = thermal expansion coefficient
Γ = boundary
γ = Petrov–Galerkin stability parameter
ε = residual error
ρ = density
Ω = computational domain
∇ = divergence operator
$\nabla\cdot$ = dot product

Presented as Paper 589 at the 44th AIAA Aerospace Sciences Meeting and Exhibit, Reno Nevada, 9–12 January 2006; received 12 January 2006; revision received 24 April 2006; accepted for publication 11 September 2006.

*Research Assistant Professor, Nevada Center for Advanced Computational Methods, 4505 Maryland Parkway, Box 454027. Member AIAA.

†Professor of Mechanical Engineering and Director, Nevada Center for Advanced Computational Methods, 4505 Maryland Parkway, Box 454027. Associate Fellow AIAA.

I. Introduction

THE finite element method (FEM) is one of the most popular numerical tools for solving thermal flow problems due to its ability to easily deal with irregular geometries, accuracy, and use of general-purpose algorithms. Adaptive FEM is especially powerful as it can provide significantly enhanced accuracy with less computational cost than using globally uniform refined and enriched meshes.

There are four main categories of adaptation: 1) h adaptation, where the element sizes vary whereas the order of the shape functions remain constant; 2) p adaptation, where the element sizes are constant whereas the orders of the shape functions increase to meet desired accuracy requirements; 3) r adaptation, where the nodes are redistributed in an existing mesh in the process of adaptation; 4) hp adaptation, which is the combination of both h and p adaptation. hp-adaptive schemes are among the best mesh-based schemes with the potential payoff of obtaining exponential convergence rates [1,2]. However, limited applications of hp-adaptive techniques for solving fluid flow problems with heat transfer are seen in the literature [3–6].

In this study, an hp-adaptive FEM is employed to solve incompressible flows with heat transfer effects. The basic methodology and adaptive strategy are presented for the numerical model. The model is validated using benchmark problems for natural convection within a differentially heated enclosure and flow with forced convective heat transfer over a backward facing step. Results are compared with published data. Natural convection within a partitioned enclosure is also examined.

II. Formulations and Solution Procedures

A. Governing Equations

The nondimensional form of the governing equations for convective thermal flow can be written as follows:
continuity equation

$$\nabla \cdot V = 0 \tag{1}$$

momentum equation

$$\frac{\partial V}{\partial t} + V \cdot \nabla V = -\nabla p + C_{\text{visc}} \nabla^2 V + C_{\text{grav}} T \tag{2}$$

energy equation

$$\frac{\partial T}{\partial t} + V \cdot \nabla T = C_T \nabla^2 T \tag{3}$$

Table 1 C_{visc}, C_T, and C_{grav} values

Convection	C_{visc}	C_T	C_{grav}
Forced	$1/Re$	$1/Pe$	0
Natural	Pr	1	$Pr\,Ra$

The corresponding values for C_{visc}, C_T, and C_{grav} are listed in Table 1 for forced and natural convection problems.

In Eqs. (1–3), the following scales and nondimensional parameters are used (Boussinesq approximation is adopted for flow with natural convective effects):

$$X = \frac{X^*}{L}, \qquad V = \frac{V^*}{\alpha/L}, \qquad p = \frac{p^*}{\rho\alpha^2/L^2}, \qquad t = \frac{t^*}{L^2/\alpha}$$
$$T = \frac{T^* - T_c}{T_h - T_c} \tag{4}$$

with Reynolds number, Rayleigh number, Prandtl number and Peclet number defined as

$$Re = \frac{\rho V L}{\mu}, \qquad Ra = \frac{g\beta(T_h - T_c)L^3}{\alpha\nu}, \qquad Pr = \frac{\nu}{\alpha}$$
$$Pe = \frac{VL}{\alpha} \tag{5}$$

B. Finite Element Formulations

Bilinear quadrilateral elements are used to initially discretize the computational domains. The Galerkin weighted residual method is employed and the variables V and T are replaced with the trial functions

$$V(\boldsymbol{x}, t) = \sum N_i(\boldsymbol{x}) V_i(t) \tag{6}$$

$$T(\boldsymbol{x}, t) = \sum N_i(\boldsymbol{x}) T_i(t) \tag{7}$$

The governing equations are solved using a projection algorithm (discussed later). Under projection decomposition, the matrix equivalent forms for the integral expressions of the governing equations are

$$[M]\{\dot{V}\} + ([K] + [A(V)])\{V\} = \{F_V\} \tag{8}$$

$$[M]\{\dot{T}\} + ([K_T] + [A(V)])\{T\} = \{F_T\} \tag{9}$$

The matrix coefficients in the finite element formulations are defined as (summation convention is implied):

$$[M] = \int_\Omega N_i N_j \,\mathrm{d}\Omega \tag{10}$$

$$A(V) = \int_\Omega N_i (N_k V_k) \frac{\partial N_j}{\partial x_j} \,\mathrm{d}\Omega \tag{11}$$

$$[K_V] = \int_\Omega C_{visc} \frac{\partial N_i \partial N_j}{\partial x_i \partial x_j} \,\mathrm{d}\Omega \tag{12}$$

$$[K_T] = \int_\Omega C_T \frac{\partial N_i \partial N_j}{\partial x_i \partial x_j} \,\mathrm{d}\Omega \tag{13}$$

Table 2 γ values

Convection	γ
Forced	$\lvert V\rvert h_e Re\, Pr$
Natural	$\lvert V\rvert h_e Ra\, Pr$

$$\{F_v\} = \int_\Omega N_i f(x_i) \,\mathrm{d}\Omega + \int_\Gamma C_{visc} N_i n_i \frac{\partial V_j}{\partial x_j} \,\mathrm{d}\Gamma \tag{14}$$

$$\{F_T\} = \int_\Omega N_i Q \,\mathrm{d}\Omega + \int_\Gamma N_i q \,\mathrm{d}\Gamma \tag{15}$$

A Petrov–Galerkin scheme is used to weight the advection terms in the governing equations. The altered weighting function skews the interpolation function in the upwind direction so that numerical dispersion can be minimized. The weighting scheme is defined as

$$W_i = N_i + \frac{\alpha h_e}{2|V|}[V \cdot \nabla N_i] \tag{16}$$

$$\alpha = \coth\frac{\gamma}{2} - \frac{2}{\gamma} \tag{17}$$

The corresponding γ values are listed in Table 2.

Mass lumping is used to obtain a fully explicit time scheme, which is easy to formulate, usually more cost effective, and better suited for parallel computation. The inverse of the mass matrix becomes

$$[M]^{-1} = \frac{1}{m_i} \tag{18}$$

C. Flow Solver

The projection algorithm, which is based on the Helmhotz–Hodge decomposition theorem, is employed as the flow solver in this study [7]. Initial work on employment of this method was conducted by Ramaswamy et al. [8]. In this method, V on Ω can be uniquely decomposed in the form

$$V = u + \nabla p \tag{19}$$

where u has zero divergence and is parallel to Γ. Applying this concept to the Navier–Stokes equations, L is applied to both sides of the equation, that is

$$L\left(\frac{\partial V}{\partial t} + \nabla P\right) = L\left[-(V \cdot \nabla)V + \frac{1}{Re}\nabla^2 V\right] \tag{20}$$

where $L(\nabla P) = 0$. Equation (20) becomes

$$\frac{\partial V}{\partial t} = -(V \cdot \nabla)V + \frac{1}{Re}\nabla^2 V \tag{21}$$

Splitting the overall velocity into two components V^* and V, the momentum equation under operator L becomes

$$\frac{V^{*n+1} - V^n}{\Delta t} + V^n \cdot \nabla V^n = \frac{1}{Re}\nabla^2 V^n \tag{22}$$

The projection of V^* is a perturbed velocity onto the divergence free space. Under the decomposition of the vector field $L(V^*)$, one can make the projection

$$V^* = V + \Delta t \nabla P \tag{23}$$

Taking the divergence on both sides of Eq. (23), and because $\nabla \cdot V = 0$, a Poisson equation for P is obtained as follows:

$$\nabla^2 P = \nabla \cdot V^* / \Delta t \tag{24}$$

In a discretized finite element representation, this can be written as

$$M(V - V^*) + \nabla P = 0 \tag{25}$$

Equation (25) can be rewritten as

$$\frac{M}{\Delta t}(V - V^*) + CP = 0 \tag{26}$$

The equation is subject to the constraint of continuity

$$C^T V = 0 \tag{27}$$

Applying mass lumping,

$$C^T M^{-1} C P = C^T V^* \tag{28}$$

eventually the velocity can be solved using the relation

$$V = V^* + \Delta t M^{-1} C P \tag{29}$$

III. Adaptive Methodology

A. Error Estimator

Choosing the right error estimator is one of the prerequisites for successfully carrying on an adaptation process. Various error estimators for adaptation exist in the literature [9–12]. In this study, an error estimator is based on an extension of the initial work by Zienkiewicz and Zhu [10]. The reason for choosing this error estimator is because of its simplicity, ease of implementation, and reasonable accuracy [10]. The estimator is commonly adopted in practical engineering analysis and adaptive procedures [9,13–16].

The basis for the error estimator stems from the error norm for linear elasticity. The error in a finite element solution can be calculated from the difference between the exact and approximate solutions, similar for the error in displacement in structural analysis:

$$e_u = u - u_{hp} \tag{30}$$

Likewise, the error for stresses can be expressed as

$$e_\sigma = \sigma - \sigma_{hp} \tag{31}$$

where u_{hp} and σ_{hp} indicates the finite element solution, whereas u and σ indicate exact solutions. Exact solutions are usually unavailable. An acceptable continuous solution can be obtained by a projection or averaging process, denoted as u^* and σ^*. Hence the error for displacement and stresses can be expressed as

$$e_u \approx u^* - u_{hp} \quad \text{and} \quad e_\sigma \approx \sigma^* - \sigma_{hp} \tag{32}$$

The errors can be expressed in certain norms such as an "energy" norm or an "L_2" norm. In this study, the "L_2" norm for corresponding stress error is defined as

$$\|e_\sigma\| = \left(\int_\Omega e_\sigma^T e_\sigma \, \mathrm{d}\Omega \right)^{1/2} \tag{33}$$

where all element errors are written as

$$\|e_\sigma\|^2 = \sum_{i=1}^{m} \|e_\sigma\|_i^2 \tag{34}$$

The error index $\eta = \eta_\sigma$ is defined in the form of error percentage:

$$\eta_\sigma = \left(\frac{\|e_\sigma\|^2}{\|\sigma^*\|^2 + \|e_\sigma\|^2} \right)^{1/2} \times 100\% \tag{35}$$

η is used to guide the adaptation procedure.

In convective heat transfer problems the errors for velocity and temperature can be expressed as

$$e_u \approx u^* - u_{hp} \quad \text{and} \quad e_T \approx T^* - T_{hp} \tag{36}$$

B. Adaptation Rules

The most important rules in adaptive FEM procedures are listed as follows: 1) 1-irregular mesh adaptation rule for h adaptation: an element is refined only if its neighbors are at the same or higher level (1-irregular mesh). This rule guarantees that multiple constraint nodes are avoided; 2) the minimum rule is followed in p adaptation: the order for an edge common for two elements never exceeds the orders of the neighboring middle nodes; 3) the adaptation rules for h and p are combined together in hp adaptation. In addition to these rules, continuity of the global basis functions are also required: this is achieved by employing constraints at the interfaces of elements supporting edge functions of different order.

C. Adaptation Strategies

Various adaptation strategies are discussed in the literature [3–6,9,13–22]. The hp-adaptive FEM strategy employed in this study follows a three step strategy and is guided by an a posteriori error estimator based on the L_2 norm. Three consecutive hp-adaptive meshes are constructed for solving the system to reach a preset target error: an initial coarse mesh, an intermediate h-adaptive mesh, and a final hp-adaptive mesh obtained by applying p-adaptive enrichments on the intermediate mesh. The p adaptation is continued when the problem solution is preasymptotic.

Both global error and local error conditions have to be met for an acceptable solution [23]. Global percentage error should not be greater than the maximum specified percentage error ($\eta \le \bar{\eta}_{\max}$). Local relative percentage error of any single element should not be greater than the averaged error among all the elements in the domain ($\|e_\sigma\|_i \le \bar{e}_{\text{avg}}$). The average element error is defined as

$$\bar{e}_{\text{avg}} = \bar{\eta}_{\max} \left[\frac{(\|\sigma^*\|^2 + \|e_\sigma\|^2)}{m} \right]^{1/2} \tag{37}$$

To decide if a local element needs to be refined, a local element refinement indicator is defined as

$$\xi_i = \frac{\|e\|_i}{\bar{e}_{\text{avg}}} \tag{38}$$

When $\xi_i > 1$ the element needs to be refined; when $\xi_i < 1$ the element needs to be unrefined. In the h-adaptive process, the new element size is calculated by using

$$h_{\text{new}} = \frac{h_{\text{old}}}{\xi_i^{1/p}} \tag{39}$$

In the p-adaptive process, the new shape function order is calculated by

$$p_{\text{new}} = p_{\text{old}} \xi_i^{1/p} \tag{40}$$

IV. Benchmark Examples

A. Natural Convection in a Square Enclosure

Natural convection within a differentially heated enclosure has been studied extensively over the past 40 years. In 1983, de Vahl Davis [24] provided accurate benchmark solutions for natural convection in a square enclosure using a finite difference stream-function/vorticity formulation with an 81×81 mesh.

In this study, the hp-adaptive algorithm was applied to natural convection within the same differentially heated square enclosure for $Ra = 10^3$–10^6. The nondimensional enclosure ($0 \le x \le 1, 0 \le y \le 1$) is heated on the left and cooled on the right, with the top and bottom walls insulated. Good agreements with benchmark data from

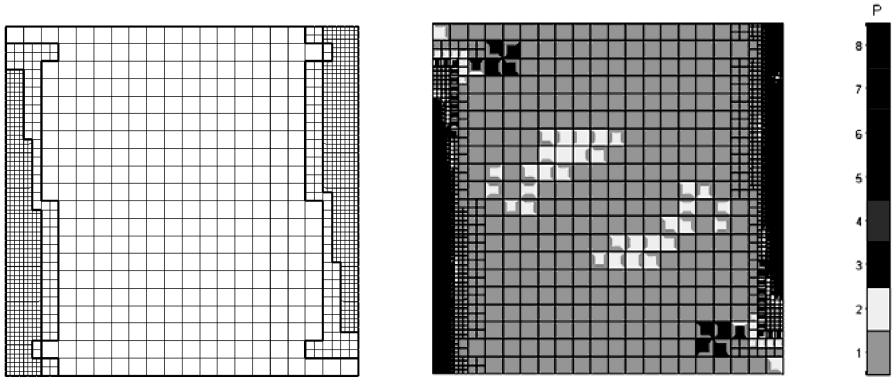

a) b)

Fig. 1 Adaptive meshes for $Ra = 10^6$: a) intermediate *h*-adaptive mesh; b) final *hp*-adaptive mesh.

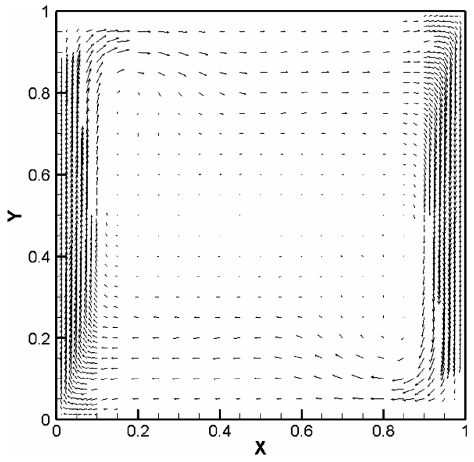

Fig. 2 Velocity vectors for $Ra = 10^6$.

de Vahl Davis [24] are obtained for the whole range of Rayleigh numbers; only the results for the highest Rayleigh number (10^6) appear in this paper.

The initial computation was based on a coarse mesh consisting of 20×20 bilinear quadrilateral elements. The intermediate *h*-adaptive mesh is shown in Fig. 1a, which was obtained after a 3-level *h* adaptation. The intermediate mesh consists of 1372 elements and 1407 degrees of freedom (DOF). The meshes are especially refined within the boundary layers. The final *hp*-adaptive mesh is shown in Fig. 1b. *p* adaptation is employed on the intermediate *h*-adaptive mesh up to 3rd order. The final *hp*-adaptive mesh consists of 1372 elements and 6529 DOF. The elements are also enriched in the boundary layers.

Steady state results are shown in Figs. 2–4 for velocity vectors, streamlines, and isotherms, respectively. Results compared with the benchmark data from de Vahl Davis [24] are listed in Table 3. The comparison data are as follows: $u_{\max}$, the maximum value of horizontal velocity component on the vertical midplane of the cavity, together with its location y; $v_{\max}$, the maximum value of vertical velocity component on the horizontal midplane of the cavity, together with its location x; Nu_0, the average Nusselt number on the heated wall; the maximum and minimum values of the local Nusselt numbers $Nu_{\max}$ and $Nu_{\min}$ on the heated side together with their locations. Excellent agreement can be observed.

B. Forced Convection in a 2-D Backward Facing Step

Two-dimensional flow over a backward facing step is a well known benchmark case that has been studied extensively over many years. The problem is easy to set up with known (expected) results at various Reynolds numbers.

In 1992, Blackwell and Pepper [25] introduced the problem of flow over a backward facing step with heat transfer as an ASME benchmark test problem. Twelve different numerical simulations were presented with fluid flow results compared against numerical flow results obtained by Gartling [26].

In this study, the *hp*-adaptive algorithm was applied to the backward facing step with heat transfer for $Re = 800$ and $Pr = 0.71$. The boundary condition settings are the same as those in Blackwell and Pepper [25]:

For inlet flow:

$$u(y) = \begin{cases} 0, & \text{for } 0 \le y \le \frac{1}{2} \\ 8y(1-2y), & \text{for } \frac{1}{2} < y \le 1 \end{cases} \tag{41}$$

$$v(y) = 0 \tag{42}$$

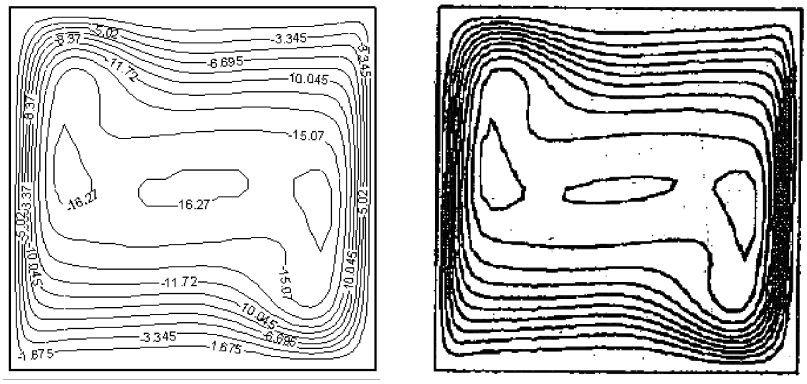

a) b)

Fig. 3 Streamlines for $Ra = 10^6$: a) *hp*-adaptive results; b) benchmark results [24]. Contours at −16.27 and −15.07 to 0 in 1.675 intervals in each case.

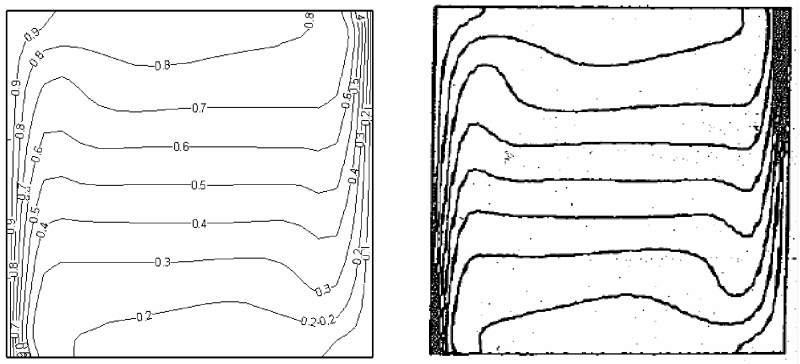

a) b)

Fig. 4 Isotherms for $Ra = 10^6$: a) *hp*-adaptive results; b) benchmark results [24]. Contours at 0 to 1 in 0.1 intervals in each case.

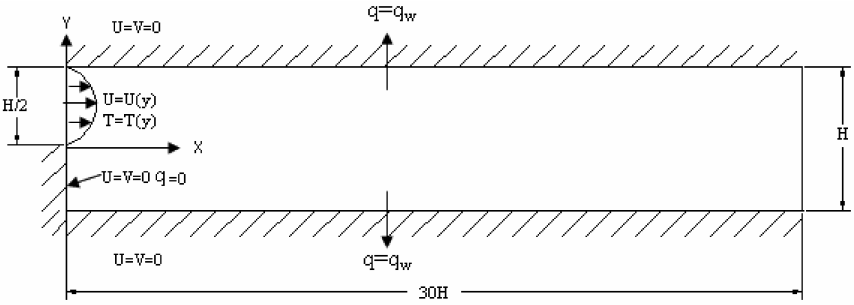

Fig. 5 Problem configuration and boundary conditions.

$$T(y) = [1 - (4y-1)^2][1 - \tfrac{1}{5}(4y-1)^2] \quad \text{for } \tfrac{1}{2} < y \le 1 \tag{43}$$

$$\frac{\partial T(y)}{\partial x} = 0 \quad \text{for } 0 \le y < \tfrac{1}{2} \tag{44}$$

On upper and lower walls

$$u(y) = v(y) = 0 \tag{45}$$

$$\nabla T \cdot \hat{n} = \frac{32}{5} \tag{46}$$

where $\hat{n}$ is the outward unit vector normal to the domain boundary. For outlet flow

$$p = 0 \tag{47}$$

At 30H, the flow has essentially returned to a fully developed profile. The heat flux can be written in terms of the Nusselt number as

$$q = (T_w - T_b)\frac{Nu_x}{2Pe} \tag{48}$$

with the local Nusselt number defined as

$$Nu_x = \frac{2Hh_x}{k} = \frac{2q''H}{[T(x)_w - T(x)_b]k} = \frac{2H}{[T(x)_w - T(x)_b]}\left.\frac{\partial T(x)}{\partial y}\right|_{y=-0.5,0.5} \tag{49}$$

where h_x is the convective heat transfer coefficient and the subscripts w and b refer to the wall and bulk quantities, respectively. The dimensionless bulk temperature is defined as

$$T(x)_b = \frac{\int u(x)T(x)\,\mathrm{d}y}{\int u(x)\,\mathrm{d}y} \tag{50}$$

The problem configuration and boundary condition settings are shown in Fig. 5.

The initial mesh consisted of 700 elements and 765 DOFs. The intermediate *h*-adaptive mesh shown in Fig. 6a consists of 4321 elements and 4275 DOFs, which is obtained after a 3-level *h* adaptation. The final *hp*-adaptive mesh was obtained for up to 3-level *p* adaptation on the intermediate *h*-adaptive mesh, which is shown in Fig. 6b (same *h*-adaptive mesh as Fig. 6a with *p* enhancement). The final mesh consists of 4321 elements and 9884 DOFs ($x : y$ ratio is 0.25).

Steady state results for stream function and temperature contours are shown in Figs. 7a and 7b, respectively.

The locations and sizes of the lower and upper wall eddies are listed in Tables 4 and 5 and compare closely with results obtained by Gartling [26]. Comparisons of velocity profiles at different cross sessions were made between the *hp*-adaptive results and benchmark data from Gartling [26], shown in Fig. 8. Temperature profiles were compared among the *hp*-adaptive results including Emery et al.'s

Table 3 Comparison of simulation results with benchmark data

Ra	$u_{\max}$ $y(x=0.5)$		$v_{\max}$ $x(y=0.5)$		Nu_0		$Nu_{\max}$ $y(x=0)$		$Nu_{\min}$ $y(x=0)$	
10^6	[24]	Present	[24]	Present	[24]	Present	[24]	Present	[24]	Present
	64.63	64.97	219.36	221.40	8.817	8.672	17.925	18.147	0.989	0.872
	0.850	0.890	0.0379	0.0381			0.037	0.042	1	1

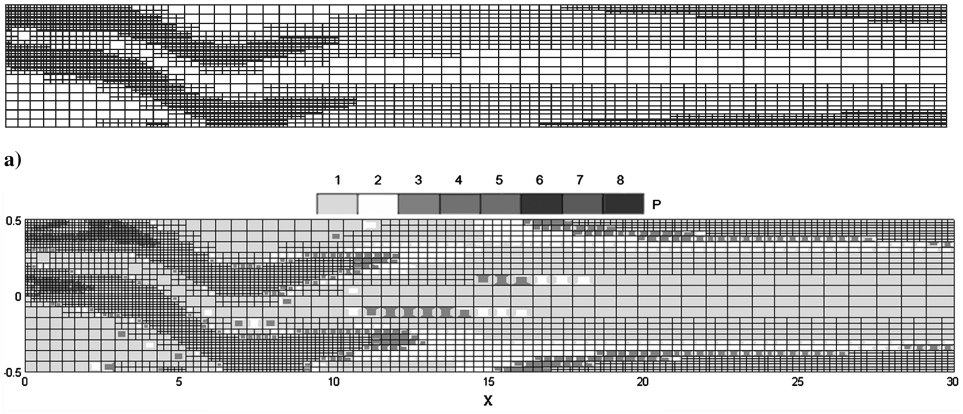

Fig. 6 Adaptive mesh: a) intermediate *h*-adaptive mesh; b) final *hp*-adaptive mesh.

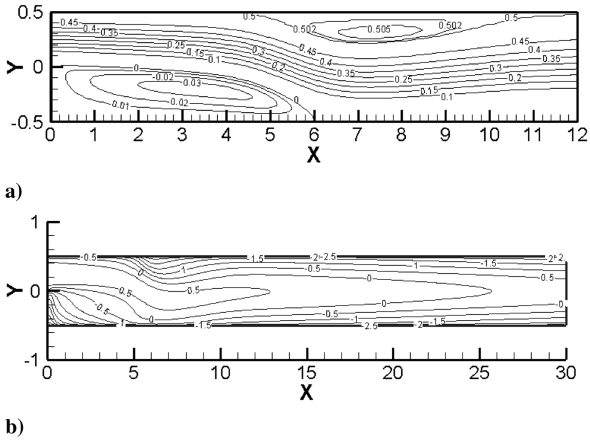

Fig. 7 Steady state solutions: a) stream function contours; b) isotherms.

from [25], as shown in Fig. 9. Excellent agreement is also observed.

However, the recirculation cell lengths are shorter compared with the benchmark solution by Gartling [26]. Also displacement exists in the v velocity, which is shown in Fig. 8b. These differences are caused by the use of Petrov–Galerkin weighting. A more detailed discussion of Petrov–Galerkin upwinding can be found in [27].

A plot of the wall Nusselt number defined in Eq. (49) is shown in Fig. 10. As the flow becomes fully developed, both upper and lower wall Nusselt numbers approach the ideal value for fully developed thermal flow in a channel, that is, as $x \to \infty$, $Nu_x \to 8.235$.

Table 4 Comparison of lower wall eddy locations and sizes with the benchmark solution by Gartling [26]

	Vortex center, x, y	Cell length, H
Benchmark	(3.35, −0.2)	6.10
Present	(3.35, −0.2)	6.00

Table 5 Comparison of upper wall eddy locations and sizes with the benchmark solution by Gartling [26]

	Vortex center, x, y	Separation, x, y	Reattachment, x, y	Cell length, H
Benchmark	(7.40, 0.30)	(4.85, 0.5)	(10.48, 0.5)	5.63
Present	(7.39, 0.31)	(4.81, 0.5)	(10.45, 0.5)	5.56

V. Application Example

Natural convection in partially divided enclosures has attracted the attention of both experimental and theoretical researchers in recent years. Practical applications include heat transfer across thermopane windows, solar collectors, fire spread and energy transfer in rooms and buildings, cooling of nuclear reactors, and heat exchanger design [28].

In many situations, a partial obstruction extends from a surface, for example, a printed circuit or a ceiling beam in a room. Research results show that the heat transfer between two heated side walls is reduced when a partial partition is present.

The partition, along with the top and bottom walls, is insulated. The left and right walls are maintained at hot and cold temperatures, respectively; in this example, $Ra = 10^4$. The problem domain is

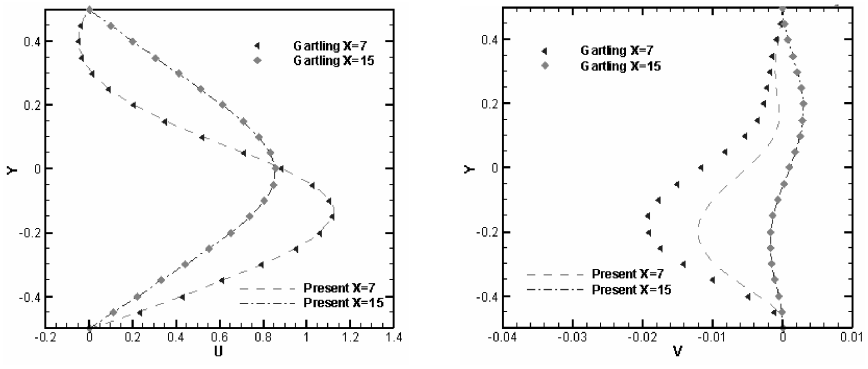

Fig. 8 Comparison of velocity profile: a) *u* compared with [26]; b) *v* compared with [26].

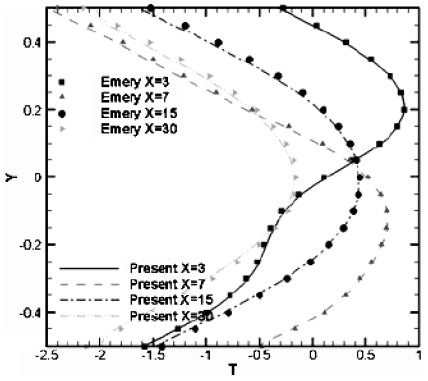

Fig. 9 Comparison of temperature profile with [25].

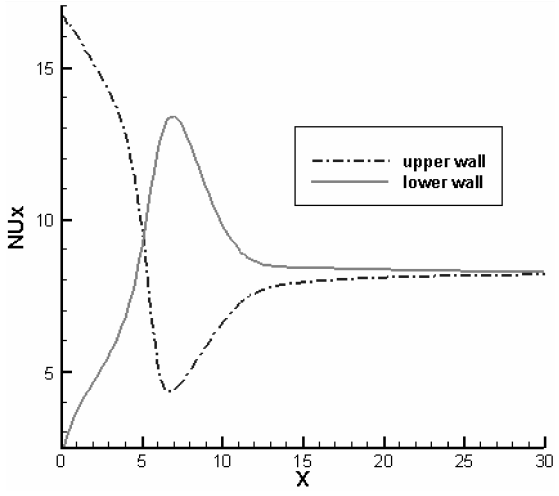

Fig. 10 Wall Nusselt number profiles.

defined as $0 \le x \le L, 0 \le y \le L$, as shown in Fig. 11. The partition thickness is $0.1L$. The height for the partition is $H = 0.3L$; the location of the partition departing from the hot wall is $d = 0.7L$.

The initial coarse mesh consisted of 388 quadrilateral elements with 435 nodes. The final mesh, which is shown in Fig. 11b, consists of 1261 elements and 4714 DOFs. The initial order for the coarse mesh is 1.

It can be seen in the final adapted mesh that the mesh is finer in the vertical boundary layers, along with higher order shape functions.

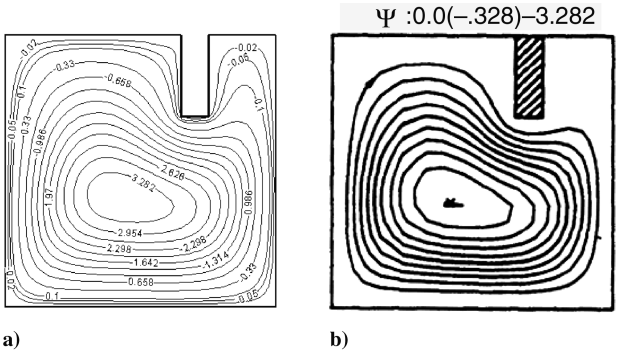

a) b)

Fig. 12 Stream functions: a) *hp*-adaptive results; b) benchmark results [29].

This occurs as a result of the flow becoming accelerated around the partition corners and along the vertical walls. The stream functions are compared with numerical simulation results obtained by Fu and Shieh [29], as shown in Fig. 12.

Steady state results for velocity vectors and temperature contours are shown in Figs. 13a and 13b respectively. Both flow and thermal patters are affected by the partition. The employment of hp-adaptive technique dynamically refines and enriches the computational mesh in the fast changing flow region.

VI. Discussion

To initially determine the computational efficiency of the adaptive algorithm, a comparison of computational times is given using a globally uniform h refined and p enriched mesh (uniformly refined up to three levels and uniform enrichment up to third order) and the hp-adaptive algorithm (adaptively refined up to three levels and enriched up to third order) for the three cases. The same maximum error level, which is $\varepsilon = 1.0 \times 10^{-7}$, was used for all the simulations. Results show that the globally h refined and p enriched algorithm consumed nearly 15, 14, and 17 times more CPU time than the hp adaptive algorithm for the three cases, as shown in Table 6. The employment of the hp adaptive algorithm results in a significant computational savings.

Generally, in convective heat transfer computational procedures, grid independent studies are needed. However, in an adaptive FEM procedure, numerically exact solutions (grid independent solutions) can be achieved using adaptive unstructured meshes [13,15]. In this study, the adaptive procedures are dynamically controlled by an L_2 norm based a posteriori error estimator, which creates an almost optimal mesh with equally distributed errors over the whole computational domain.

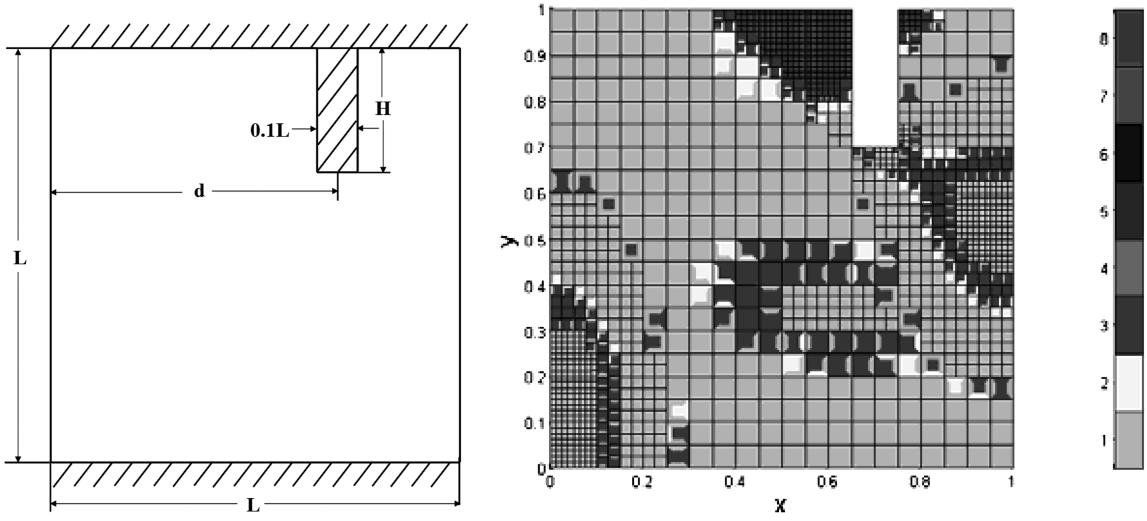

a) b)

Fig. 11 Partial divided enclosure: a) configuration; b) final *hp*-adaptive mesh.

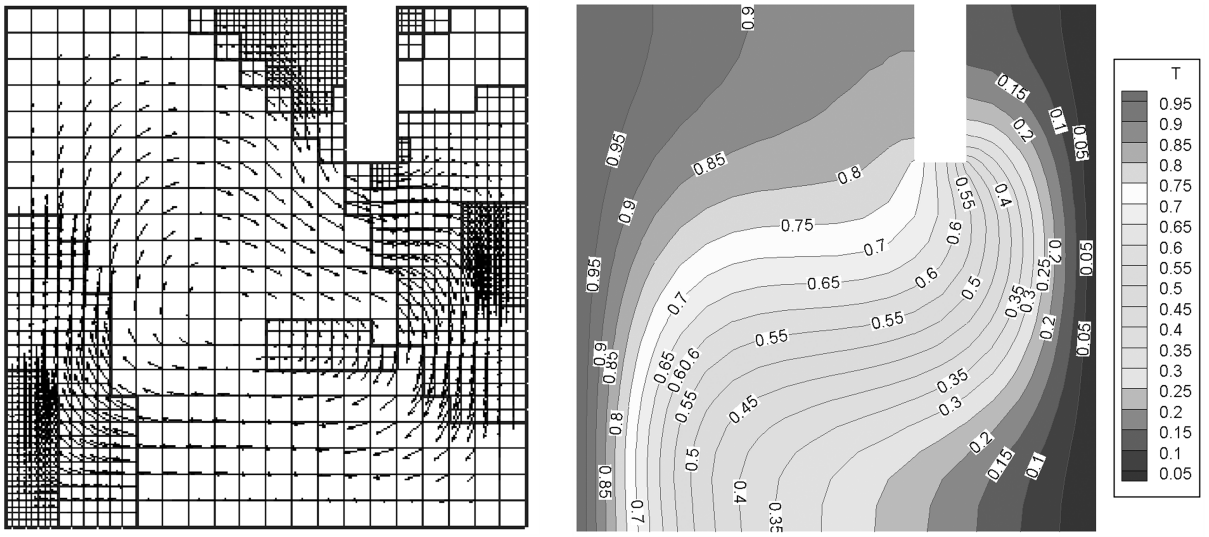

a) b)

Fig. 13 Simulation results: a) velocity vectors; b) isotherms.

Table 6 CPU time comparison between uniform refined and enriched algorithm and *hp*-adaptive algorithm

Compare cases	No. of element		No. of DOF		Total CPU time, s	Per DOF CPU time, sec/DOF
	Initial	Final	Initial	Final		
Uniform h and p FEM, case 1	6,400	6,400	58,081	58,081	598,815	10.31
hp-adaptive FEM, case 1	400	1,372	441	6,529	38,782	5.94
Uniform h and p FEM, case 2	11,200	11,200	101,569	101,569	790,206	7.78
hp-adaptive FEM, case 2	700	4,321	765	9,884	55,943	5.66
Uniform h and p FEM, case 3	6,208	6,208	56,425	56,425	376,354	6.67
hp-adaptive FEM, case 3	388	1,261	435	4,714	21,307	4.52

VII. Conclusions

There are basically two ways to improve computational accuracy: 1) use a fine mesh or 2) employ high order shape functions. In this study, an hp-adaptive finite element technique, which can dynamically control mesh size and shape function order, has been developed. The hp-adaptive algorithm uses both mesh refinement (h) and increasing spectral order (p). In h adaptation, a major disadvantage is the complexity of handling constraint nodes, which can cause an irregular mesh; however, an overdistorted mesh can be avoided compared with using r adaptation. In p adaptation, high accurate results are generally expected, but such methods are generally not as efficient as combined hp methods.

The hp-adaptive finite element technique has been applied to both forced and natural convection problems. Thermal problems such as natural convection in a square enclosure, forced convection heat transfer associated with flow downstream of a backward facing step, and natural convection in a partition enclosure are investigated. Results agree well with data in the literature. The hp-adaptive algorithm generates very accurate results and reduces the overall computational effort compared with globally refined and enriched meshes attempting to achieve similar residual errors.

The hp-adaptive algorithm is also being applied to solve both atmospheric and indoor contaminant transport problems [30,31]. Preliminary results indicate that the hp-adaptive algorithm is effective for environmental fluid dynamics, heat and mass transport problems; the use of adaptive techniques also appears attractive for use in homeland security and emergency response related situations [32].

References

[1] Guo, B., and Babuska, I., "The $h-p$ Version of the Finite Element Method, Part 1," *Computational Mechanics*, Vol. 1, No. 1, 1986, pp. 21–21; Guo, B., and Babuska, I., "The $h-p$ Version of the Finite Element Method, Part 2," *Computational Mechanics*, Vol. 1, No. 3, 1986, pp. 203–220.

[2] Gui, W., and Babuska, I., "The h, p, and $h-p$ Version of the Finite Element Method in One Dimension, Part 1," *Numerische Mathematik*, Vol. 49, No. 6, 1986, pp. 577–612; Gui, W., and Babuska, I., "The h, p, and $h-p$ Version of the Finite Element Method in One Dimension, Part 2," *Numerische Mathematik*, Vol. 49, No. 6, 1986, pp. 613–657; Gui, W., and Babuska, I., "The h, p, and $h-p$ Version of the Finite Element Method in One Dimension, Part 3," *Numerische Mathematik*, Vol. 49, No. 6, 1986, pp. 659–683.

[3] Oden, J. T., Wu, W., and Ainsworth, W., "Three-Step H–P Adaptive Strategy for the Incompressible Navier–Stokes Equations," *Modeling, Mesh Generation, and Adaptive Numerical Methods for Partial Differential Equations*, Vol. 75, Springer–Verlag, New York, 1995, pp. 347–366.

[4] Devloo, P., Oden, J. T., and Pattani, P., "An $h-p$ Adaptive Finite Element Method for the Numerical Simulation of Compressible Flow," *Computer Methods in Applied Mechanics and Engineering*, Vol. 70, No. 2, 1988, pp. 203–235.

[5] Oden, J. T., and Demkowicz, L., "$h-p$ Adaptive Finite Element Methods in Computational Fluid Dynamics," *Computer Methods in Applied Mechanics and Engineering*, Vol. 89, No. 1–3, 1991, pp. 11–40.

[6] Oden, J. T., Kennon, S. R., Tworzydlo, W. W., Bass, J. M., and Berry, C., "Progress on Adaptive hp-Finite Element Methods for the Incompressible Navier–Stokes Equations," *Computational Mechanics*, Vol. 11, No. 5–6, 1993, pp. 421–432.

[7] Chorin, A. J., "Numerical Solution of the Navier–Stokes Equations," *Mathematics of Computation*, Vol. 22, No. 104, 1968, pp. 745–762.

[8] Ramaswamy, B., Jie, T. C., and Akin, J. E., "Semi-Implicit and Explicit Finite Element Schemes for Coupled Fluid/Thermal Problems," *International Journal for Numerical Methods in Engineering*, Vol. 34, No. 2, 1992, pp. 675–696.

[9] Nithiarasu, P., and Zienkiewicz, O. C., "Adaptive Mesh Generation for Fluid Mechanics Problems," *International Journal for Numerical Methods in Engineering*, Vol. 47, No. 1, 2000, pp. 629–662.

[10] Zienkiewicz, O. C., and Zhu, R. J. Z., "A Simple Error Estimator and Adaptive Procedure for Practical Engineering Analysis," *International Journal for Numerical Methods in Engineering*, Vol. 24, No. 2, 1987, pp. 337–357.

[11] Oden, J. T., Demkowicz, L., Rachowicz, W., and Westermann, T. A., "Toward a Universal $h-p$ Adaptive Finite Element Strategy, Part 2: A Posteriori Error Estimation," *Computer Methods in Applied Mechanics and Engineering*, Vol. 77, No. 1–2, 1989, pp. 113–180.

[12] Ainsworth, M., and Oden, J. T., "A Posteriori Error Estimation in Finite Element Analysis, Pure and Applied Mathematics," *Wiley–Interscience Series of Texts, Monographs and Tracts*, Wiley, New York, 2000.

[13] Hetu, J. F., and Pelletier, D. H., "Fast, Adaptive Finite Element Scheme for Viscous Incompressible Flows," *AIAA Journal*, Vol. 30, No. 11, 1992, pp. 2677–2682.

[14] Pelletier, D., Hetu, J.-F., and Ilinca, F., "Adaptive Finite Element Method for Thermal Flow Problems," *AIAA Journal*, Vol. 32, No. 4, 1994, pp. 741–747.

[15] Nithiarasu, P., "An Adaptive Remeshing Technique for Laminar Natural Convection Problems," *Heat and Mass Transfer*, Vol. 38, No. 3, 2002, pp. 243–250.

[16] Bose, A., "Parallel p-Adaptive Finite Element Methods for Viscous Incompressible Non-Newtonian Flows," Doctoral Thesis, Univ. of Texas at Austin, 1997.

[17] Singh, M., "Object-Oriented Implementation of p-Adaptive Finite Element Method," Doctoral Thesis, Rice Univ., 1999.

[18] Peraire, J., Vahdati, M., Morgan, K., and Zienkiewicz, O. C., "Adaptive Remeshing for Compressible Flows," *Journal of Computational Physics*, Vol. 72, No. 2, 1987, pp. 449–466.

[19] Rachowicz, W., Oden, J. T., and Demkowicz, L., "Toward a Universal $h-p$ Adaptive Finite Element Strategy, Part 3: Design of $h-p$ Meshes," *Computer Methods in Applied Mechanics and Engineering*, Vol. 77, No. 1–2, 1989, pp. 181–212.

[20] Ainsworth, M., and Senior, B., "Aspects of an Adaptive hp-Finite Element Method: Adaptive Strategy, Conforming Approximation, and Efficient Solvers," *Computer Methods in Applied Mechanics and Engineering*, Vol. 150, No. 1–4, 1997, pp. 65–87.

[21] Ainsworth, M., and Senior, B., "An Adaptive Refinement Strategy for hp-Finite Element Computations," *Applied Numerical Mathematics*, Vol. 26, No. 1–2, 1998, pp. 165–178.

[22] Demkowicz, L., Rachowicz, W., and Devloo, Ph., "A Fully Automatic hp-Adaptivity," *Journal of Scientific Computing*, Vol. 17, Nos. 1–4, Dec. 2002, pp. 127–155.

[23] Onate, E., and Bugeda, G., "Mesh Optimality Criteria for Adaptive Finite Element Computations," *The Mathematics of Finite Elements and Applications*, Wiley, Chichester, England, 1994, pp. 121–135, Chap. 7.

[24] De Vahl Davis, G., "Natural Convection of Air in a Square Cavity: A Bench Mark Numerical Solution," *International Journal for Numerical Methods in Fluids*, Vol. 3, No. 3, 1983, pp. 249–264.

[25] Blackwell, B. G., and Pepper, D. W., *Benchmark Problems for Heat Transfer Codes*, HTD-Vol. 222, American Society of Mechanical Engineers, New York, 1992.

[26] Gartling, D. K., "A Test Problem for Outflow Boundary Conditions: Flow over a Backward-Facing Step," *International Journal for Numerical Methods in Fluids*, Vol. 11, 1990, pp. 953–967.

[27] Brooks, A. N., "Streamline Upwind/Petrov–Galerkin Formulations for Convection Dominated Flows with Particular Emphasis on the Incompressible Navier–Stokes Equations," *Computer Methods in Applied Mechanics and Engineering*, Vol. 32, No. 1–3, 1982, pp. 199–259.

[28] Chen, K. S., Ku, A. C., and Chou, C. H., "Investigation of Natural Convection in Partially Divided Rectangular Enclosures Both With and Without an Opening in the Partition Plate: Measurements," *Journal of Heat Transfer*, Vol. 112, No. 3, 1990, pp. 648–652.

[29] Fu, W. S., and Shieh, W. J., "A Penalty Finite Element Method for Natural Convection Heat Transfer in a Partially Divided Enclosure," *International Communications in Heat and Mass Transfer*, Vol. 15, No. 3, 1998, pp. 323–332.

[30] Wang, X., and Pepper, D. W., "A Hybrid Numerical Model for Simulating Environmental Dispersion," *Proceedings of Energy Conversion and Resources 2005*, Vol. 2005, American Society of Mechanical Engineers, New York, 2005, pp. 53–60.

[31] Wang, X., and Pepper, D. W., "Simulation of Heat, Mass, and Momentum Transfer Within Building Interiors," *Proceedings of the American Society of Mechanical Engineers Summer Heat Transfer Conference*, Vol. 3, American Society of Mechanical Engineers, New York, 2005, pp. 859–864.

[32] Pepper, D. W., and Wang, X., "A Hybrid Numerical Model for Quickly Assessing Indoor Contaminant Transport," *The Built Environment*, Vol. 82, WIT Press, Southampton, U.K., 2005, pp. 53–62.